Contents list available at ScienceDrect

Pattern Recognition

journal homepage: www.elsevier.com/locate/pr

Computing internally constrained motion of 3-D sensor data for motion interpretation

Kenichi Kanatani[a,*], Chikara Matsunaga

[a] Department of Computer Science, Okayama University, Okayama 700-8530, Japan [b] Sakura R&D Center, FOR-A Co., Ltd., Sakura, Chiba 285-0802, Japan

ARTICLE INFO

Article history:
Received 10 September 2012
Received in revised form
2 November 2012
Accepted 24 November 2012
Available online 3 December 2012

Keywords:
3-D affinity
3-D similarity
3-D rigid motion
Internal constraints
Geometric model selection
Stereo vision
Geodetic sensing

ABSTRACT

Given 3-D sensor data of points slightly moving in space, we consider the problem of discerning whether or not translation, rotation, and scale change take place and to what extent. For this purpose, we propose a new method for fitting various motion models to 3-D sensor data. Based on the observation that subgroups of 3-D affinity are defined by imposing various internal constraints on the parameters, our method fits 3-D affinity with internal constraints using the scheme of EFNS, which, unlike conventional methods, dispenses with any particular parameterizations for particular motion models. Then, we apply our method to simulated stereo vision data for motion interpretation, using various model selection criteria. We also apply our method to the GPS geodetic data of the land deformation in northeast Japan, where a massive earthquake took place on 11 March 2011. It is expected that our proposed technique will be widely used for 3-D analysis involving hierarchical motion models in various domains including computer vision, robotic navigation, and geodetic science.

1. Introduction

Suppose multiple points are slightly moving in space and we measure their 3-D positions before and after the motion, using 3-D sensors such as stereo vision and range finders. We consider the problem of discerning what type of motion is taking place, e.g., translation, rotation, scale change, or all. A different interpretation is: for measuring the 3-D positions of stationary points by two different 3-D sensors, are they correctly calibrated? If not, is there sensor misalignment of translation, rotation, scale, or all? For this, we postulate different motion models such as translation, rotation, and scale change, fit each model to the observed data, and judge which model best explains them. To this end, we need to fit each candidate model to the observation, but different models have different sets of parameters. For example, the translation model requires only the x, y, and z components of the translation, but if rotations are involved, we need to introduce some parameters such as Euler angles, quaternions, and Lie algebra parameters [4].

In the past, different parameterizations were combined with different optimization techniques that best suit them. For example, 3-D rotation was parameterized by quaternions [21], which was optimized by the *FNS* (*Fundamental Numerical Scheme*) of Chojnacki et al. [2], and 3-D similarity was parameterized by extended quaternions and a translation vector, which were optimized by the Gauss-Helmert method [13]. Since the residual, i.e., the cost function to be minimized, has a different form for different parameterization with different derivative expressions, a different minimization technique is required for each model.

This paper proposes a *unified* approach for fitting different models by exploiting the hierarchical structure of the motion models. We note that translation, rotation, scale change, and their combinations define subgroups of the group of affine transformations, or affinity for short, and that different subgroups are associated with different internal constraints. By *internal* constraints, we mean the condition that the motion must satisfy *irrespective of observation data*; if observation is involved, the constraints are *external*. For optimization with internal constraints, we adopt the *EFNS* (*Extended FNS*) of Kanatani and Sugaya [15]. This is a method for computing the so-called "fundamental matrix [3] " $\mathbf{F}$ for 3-D analysis from two images. The fundamental matrix $\mathbf{F}$ must satisfy not only the external constraint called the "epipolar equation" but also the internal constraint $\det \mathbf{F} = 0$. If the internal constraint is disregarded, $\mathbf{F}$ is easily computed by the FNS of Chojnacki et al. [2]. The EFNS is an extension to the FNS so that the internal constraint is automatically satisfied at the end of the iterations. However, the EFNS can deal with only a single scalar external constraint, such as the epipolar equation, but affinity and their subgroups are

* Corresponding author. Tel./fax: +81 86 251 8173..
E-mail addresses: kanatani@suri.cs.okayama-u.ac.jp (K. kanatani), matsunaga@for-a.co.jp (C. Matsunaga).

0131-3203/$–see front matter ©2012 Elsevier Ltd.
yttp://dx.doi.org/10.1016/j.patcog.2012.11.023

described by 3-D vector equations. In this paper, we extend the EFNS to multiple external constrains.

Section 2 gives a mathematical formulation of 3-D affinity and its internal constraints. Section 3 describes the principle of maximum likelihood (ML) that takes inhomogeneous and anisotropic uncertainty of 3-D sensor data into consideration. In Section 4, we present our optimization procedure in the presence of internal constraints without using any particular parameterization. In Section 5, we show simulated stereo vision experiments to show how to interpret the motion using various model selection criteria. In Section 6, we apply our method to the GPS geodetic data of the land deformation in northeast Japan, where a massive earthquake took place on 11 March 2011. In Section 7, we conclude that our proposed technique is expected to play an important role in various domains such as computer vision, robotic navigation, and geodetic science.

2. 3-D affinity and internal constraints

Let $\mathbf{r} = (x, y, z)^\top$ and $\mathbf{r}' = (x', y', z')^\top$ be, respectively, the 3-D positions of a generic point before and after a motion. The motion is *affine* if

$$\mathbf{r}' = \mathbf{A}\mathbf{r} + \mathbf{t}, \tag{1}$$

for some nonsingular matrix $\mathbf{A}$ and a translation vector $\mathbf{t}$. We place no restriction on the magnitude of the motion, i.e., the motion can be arbitrarily large. As described in Introduction, we intend to use our method to interpret small motions, but this is only for application perspective; the subsequent theory and procedure apply to any motion.

We write the elements of the matrix $\mathbf{A}$ and the vector $\mathbf{t}$ as

$$\mathbf{A} = \begin{pmatrix} u_1 & u_2 & u_3 \\ u_4 & u_5 & u_6 \\ u_7 & u_8 & u_9 \end{pmatrix}, \qquad \mathbf{t} = \begin{pmatrix} u_{10}L_0 \\ u_{11}L_0 \\ u_{12}L_0 \end{pmatrix}, \tag{2}$$

where L_0 is a reference length having the same order as $\mathbf{r}$ and $\mathbf{r}'$. Using such a reference length is equivalent to using a unit of length such that the components of $\mathbf{r}$ and $\mathbf{r}'$ have order 1; this stabilizes numerical computation with finite length. We can write (1) as

$$\begin{aligned} u_0 x' &= u_1 x + u_2 y + u_3 z + u_{10} L_0, \\ u_0 y' &= u_4 x + u_5 y + u_6 z + u_{11} L_0, \\ u_0 z' &= u_7 x + u_8 y + u_9 z + u_{12} L_0, \end{aligned} \tag{3}$$

where we let $u_0 = 1$. Introducing this dummy u_0 and regarding (1) as *homogeneous* linear equations in the parameters is the "key" to our method. If we define 13-D vectors $\mathbf{u}$, $\boldsymbol{\xi}^{(1)}$, $\boldsymbol{\xi}^{(2)}$, and $\boldsymbol{\xi}^{(3)}$ by

$$\begin{aligned} \mathbf{u} &= (u_1, u_2, u_3, u_4, u_5, u_6, u_7, u_8, u_9, u_{10}, u_{11}, u_{12}, u_0)^\top, \qquad (4) \\ \boldsymbol{\xi}^{(1)} &= (x/L_0, y/L_0, z/L_0, 0, 0, 0, 0, 0, 0, 1, 0, 0, -x'/L_0)^\top, \\ \boldsymbol{\xi}^{(2)} &= (0, 0, 0, x/L_0, y/L_0, z/L_0, 0, 0, 0, 0, 1, 0, -y'/L_0)^\top, \\ \boldsymbol{\xi}^{(3)} &= (0, 0, 0, 0, 0, 0, x/L_0, y/L_0, z/L_0, 0, 0, 1, -z'/L_0)^\top, \qquad (5) \end{aligned}$$

we can write (3) as

$$(\boldsymbol{\xi}^{(1)}, \mathbf{u}) = 0, \qquad (\boldsymbol{\xi}^{(2)}, \mathbf{u}) = 0, \qquad (\boldsymbol{\xi}^{(3)}, \mathbf{u}) = 0, \tag{6}$$

where and hereafter we denote by $(\mathbf{a}, \mathbf{b})$ the inner product of vectors $\mathbf{a}$ and $\mathbf{b}$.

Subgroups of 3-D affinity can be specified by imposing appropriate internal constraints $\phi_1(\mathbf{u}) = 0$, ..., $\phi_r(\mathbf{u}) = 0$, where $\phi_1(\mathbf{u})$, ..., $\phi_r(\mathbf{u})$ are *homogeneous polynomials*.

Example 1. Note that (3) defines a rigid motion if $\mathbf{A}$ is a rotation matrix. A matrix represents a rotation if and only if the three columns are mutually orthogonal unit vectors. It represents a reflection if its determinant is negative, but we do not consider the sign, since we are fitting a motion model to given sensor data. Thus, a rigid motion is specified by the following *quadratic forms*:

$$\begin{aligned} &\phi_1(\mathbf{u}) = u_1u_4 + u_2u_5 + u_3u_6, \qquad \phi_2(\mathbf{u}) = u_4u_7 + u_5u_8 + u_6u_9, \\ &\phi_3(\mathbf{u}) = u_7u_1 + u_8u_2 + u_9u_3, \\ &\phi_4(\mathbf{u}) = u_1^2 + u_2^2 + u_3^2 - u_4^2 - u_5^2 - u_6^2, \\ &\phi_5(\mathbf{u}) = u_4^2 + u_5^2 + u_6^2 - u_7^2 - u_8^2 - u_9^2, \\ &\phi_6(\mathbf{u}) = u_1^2 + u_2^2 + u_3^2 - u_0^2. \end{aligned} \tag{7}$$

If $\phi_6(\mathbf{u}) = 0$ is removed, the matrix $\mathbf{A}$ is a scalar multiple of a rotation matrix and hence (3) represents a similarity.

Example 2. The motion is identity if $\mathbf{A} = \mathbf{I}$ and $\mathbf{t} = \mathbf{0}$. This is specified by the following *linear forms*:

$$\begin{aligned} &\phi_7(\mathbf{u}) = u_2, \quad \phi_8(\mathbf{u}) = u_3, \quad \phi_9(\mathbf{u}) = u_4, \quad \phi_{10}(\mathbf{u}) = u_6, \\ &\phi_{11}(\mathbf{u}) = u_7, \quad \phi_{12}(\mathbf{u}) = u_8, \quad \phi_{13}(\mathbf{u}) = u_1 - u_5, \\ &\phi_{14}(\mathbf{u}) = u_5 - u_9, \quad \phi_{15}(\mathbf{u}) = u_1 - u_0, \quad \phi_{16}(\mathbf{u}) = u_{10}, \\ &\phi_{17}(\mathbf{u}) = u_{11}, \quad \phi_{18}(\mathbf{u}) = u_{12}. \end{aligned} \tag{8}$$

If $\phi_{15}(\mathbf{u}) = 0$ is removed, the matrix $\mathbf{A}$ is a scalar multiple of the identity $\mathbf{I}$, and hence (3) represents a scale change. If $\phi_{16}(\mathbf{u}) = 0$, $\phi_{17}(\mathbf{u}) = 0$, and $\phi_{18}(\mathbf{u}) = 0$ are removed, (3) represents a translation.

The domain $\mathcal{U}$ of $\mathbf{u}$ that satisfies internal constraints $\phi_1(\mathbf{u}) = 0$, ..., $\phi_r(\mathbf{u}) = 0$ is an algebraic variety in $\mathcal{R}^{13}$. We can ignore the convention $u_0 = 1$, because the solution $\mathbf{u}$ of (6) has scale indeterminacy. Hereafter, we regard $\mathbf{u}$ as a unit vector ($\|\mathbf{u}\| = 1$); we renormalize it to $u_0 = 1$ in the final stage of evaluating $\mathbf{A}$ and $\mathbf{t}$. Thus, the domain $\mathcal{U}$ of $\mathbf{u}$ is written as

$$\mathcal{U} = \{\mathbf{u} \,|\, \|\mathbf{u}\| = 1, \phi_1(\mathbf{u}) = 0, ..., \phi_r(\mathbf{u}) = 0\} \subset \mathcal{R}^{13}. \tag{9}$$

Since $\mathcal{U}$ is the intersection of the unit sphere $\|\mathbf{u}\| = 1$ with the r hypersurfaces defined by $\phi_k(\mathbf{u}) = 0$, $k = 1, ..., r$, it is a $(12 - r)$-D variety. Consider the surface normals to $\mathcal{U}$. The surface normal to the unit sphere $\|\mathbf{u}\| = 1$ is $\mathbf{u}$ itself. Each hypersurface $\phi_k(\mathbf{u}) = 0$ has surface normal $\nabla_{\mathbf{u}}\phi_k$. It follows that all the surface normals to $\mathcal{U}$ constitute a linear space

$$\mathcal{N}_{\mathbf{u}} = \{\mathbf{u}, \nabla_{\mathbf{u}}\phi_1, ..., \nabla_{\mathbf{u}}\phi_r\}_{\mathcal{L}}, \tag{10}$$

where $\{\cdots\}_{\mathcal{L}}$ denotes the linear space spanned by $\cdots$. If we define

$$\mathcal{M}_{\mathbf{u}} = \{\nabla_{\mathbf{u}}\phi_1, ..., \nabla_{\mathbf{u}}\phi_r\}_{\mathcal{L}}, \tag{11}$$

the space $\mathcal{N}_{\mathbf{u}}$ is decomposed into the direct sum

$$\mathcal{N}_{\mathbf{u}} = \{\mathbf{u}\}_{\mathcal{L}} \oplus \mathcal{M}_{\mathbf{u}}. \tag{12}$$

The "core" of our EFNS procedure is the following lemma:

Lemma 1. $\phi_k(\mathbf{u}) = 0 \Longleftrightarrow (\nabla_{\mathbf{u}}\phi_k, \mathbf{u}) = 0$

Proof. If $\phi_k(\mathbf{u})$ is a homogeneous polynomial of degree D_k, we have $\phi_k(t\mathbf{u}) = t^{D_k}\phi_k(\mathbf{u})$ for arbitrary t. Differentiation on both sides with respect to t yields $(\nabla_{\mathbf{u}}\phi_k(t\mathbf{u}), \mathbf{u}) = D_k t^{D_k-1}\phi_k(\mathbf{u})$. Letting $t = 1$, we obtain $(\nabla_{\mathbf{u}}\phi_k, \mathbf{u}) = D_k\phi_k(\mathbf{u})$. □

Thus, the domain $\mathcal{U}$ in (9) can be alternatively written as

$$\mathcal{U} = \{\mathbf{u} \,|\, \|\mathbf{u}\| = 1, \mathbf{u} \in \mathcal{M}_{\mathbf{u}}^{\perp}\}, \tag{13}$$

where $\perp$ denotes orthogonal complement.

3. Maximum likelihood estimation

Let $\mathbf{r}_\alpha$ and $\mathbf{r}'_\alpha$, $\alpha = 1, ..., N$, be, respectively, the measurements of N points moving in space before and after their motion. Unlike 2-D data, 3-D sensor data often have large inhomogeneous and anisotropic uncertainty. We model this uncertainty by independent Gaussian noise of mean $\mathbf{0}$ and covariance matrices $\sigma^2 V_0[\mathbf{r}_\alpha]$ and $\sigma^2 V_0[\mathbf{r}'_\alpha]$, where σ, which we call the *noise level*, describes the magnitude of the noise, while $V_0[\mathbf{r}_\alpha]$ and $V_0[\mathbf{r}'_\alpha]$, which we call the

normalized covariance matrices, describe the directional dependence of the noise distribution of each measurement. We assume that the noise level σ is unknown but the normalized covariance matrices $V_0[\mathbf{r}_\alpha]$ and $V_0[\mathbf{r}'_\alpha]$ are known. This separation is merely a convenience, reflecting the fact that the absolute magnitude of noise is difficult to estimate, while maximum likelihood estimation, as shown shortly, can be done only using $V_0[\mathbf{r}_\alpha]$ and $V_0[\mathbf{r}'_\alpha]$.

Let $\boldsymbol{\xi}_\alpha^{(k)}$ be the values of $\boldsymbol{\xi}^{(k)}$ in (5) computed from $\mathbf{r}_\alpha$ and $\mathbf{r}'_\alpha$. From (5), the perturbations $\Delta\boldsymbol{\xi}_\alpha^{(k)}$ of $\boldsymbol{\xi}_\alpha^{(k)}$ are related to the perturbations Δx_α, Δy_α, Δz_α, $\Delta x'_\alpha$, $\Delta y'_\alpha$, $\Delta z'_\alpha$ of the original data x_α, y_α, z_α, x'_α, y'_α, and z'_α in the form

$$\Delta\boldsymbol{\xi}_\alpha^{(1)} = \mathbf{T}_1^\top \begin{pmatrix} \Delta x_\alpha \\ \Delta y_\alpha \\ \Delta z_\alpha \\ \Delta x'_\alpha \\ \Delta y'_\alpha \\ \Delta z'_\alpha \end{pmatrix}, \quad \Delta\boldsymbol{\xi}_\alpha^{(2)} = \mathbf{T}_2^\top \begin{pmatrix} \Delta x_\alpha \\ \Delta y_\alpha \\ \Delta z_\alpha \\ \Delta x'_\alpha \\ \Delta y'_\alpha \\ \Delta z'_\alpha \end{pmatrix}, \quad \Delta\boldsymbol{\xi}_\alpha^{(3)} = \mathbf{T}_3^\top \begin{pmatrix} \Delta x_\alpha \\ \Delta y_\alpha \\ \Delta z_\alpha \\ \Delta x'_\alpha \\ \Delta y'_\alpha \\ \Delta z'_\alpha \end{pmatrix}, \tag{14}$$

where we define

$$\mathbf{T}_1 = \frac{1}{L_0}\begin{pmatrix} \mathbf{I} & \mathbf{O} & \mathbf{O} & \mathbf{O} & \mathbf{0} \\ \mathbf{O} & \mathbf{O} & \mathbf{O} & \mathbf{O} & -\mathbf{i} \end{pmatrix}, \quad \mathbf{T}_2 = \frac{1}{L_0}\begin{pmatrix} \mathbf{O} & \mathbf{I} & \mathbf{O} & \mathbf{O} & \mathbf{0} \\ \mathbf{O} & \mathbf{O} & \mathbf{O} & \mathbf{O} & -\mathbf{j} \end{pmatrix},$$
$$\mathbf{T}_3 = \frac{1}{L_0}\begin{pmatrix} \mathbf{O} & \mathbf{O} & \mathbf{I} & \mathbf{O} & \mathbf{0} \\ \mathbf{O} & \mathbf{O} & \mathbf{O} & \mathbf{O} & -\mathbf{k} \end{pmatrix}. \tag{15}$$

Here, $\mathbf{O}$ and $\mathbf{0}$ denote submatrices and columns consisting of 0 of appropriate dimensions (which are easily understood), and we put $\mathbf{i} = (1,0,0)^\top$, $\mathbf{j} = (0,1,0)^\top$, and $\mathbf{k} = (0,0,1)^\top$. We define the covariance matrix between $\boldsymbol{\xi}_\alpha^{(k)}$ and $\boldsymbol{\xi}_\alpha^{(l)}$ by

$$\sigma^2 V_0^{(kl)}[\boldsymbol{\xi}_\alpha] = E[\Delta\boldsymbol{\xi}_\alpha^{(k)}\Delta\boldsymbol{\xi}_\alpha^{(l)\top}] = \sigma^2 \mathbf{T}_k^\top \begin{pmatrix} V_0[\mathbf{r}_\alpha] & \mathbf{O} \\ \mathbf{O} & V_0[\mathbf{r}'_\alpha] \end{pmatrix} \mathbf{T}_l, \tag{16}$$

where $E[\,\cdot\,]$ denotes expectation over data uncertainty.

Let $\bar{\boldsymbol{\xi}}_\alpha^{(k)}$ be the true values of the observations $\boldsymbol{\xi}_\alpha^{(k)}$. Under our noise model, *maximum likelihood* (*ML*) estimation is equivalent to minimizing the Mahalanobis distance, hereafter simply called the *residual*,

$$J = \sum_{\alpha=1}^{N} \left(\begin{pmatrix} \boldsymbol{\xi}_\alpha^{(1)} - \bar{\boldsymbol{\xi}}_\alpha^{(1)} \\ \boldsymbol{\xi}_\alpha^{(2)} - \bar{\boldsymbol{\xi}}_\alpha^{(2)} \\ \boldsymbol{\xi}_\alpha^{(3)} - \bar{\boldsymbol{\xi}}_\alpha^{(3)} \end{pmatrix}, \begin{pmatrix} V_0^{(11)}[\boldsymbol{\xi}_\alpha] & V_0^{(12)}[\boldsymbol{\xi}_\alpha] & V_0^{(13)}[\boldsymbol{\xi}_\alpha] \\ V_0^{(21)}[\boldsymbol{\xi}_\alpha] & V_0^{(22)}[\boldsymbol{\xi}_\alpha] & V_0^{(23)}[\boldsymbol{\xi}_\alpha] \\ V_0^{(31)}[\boldsymbol{\xi}_\alpha] & V_0^{(32)}[\boldsymbol{\xi}_\alpha] & V_0^{(33)}[\boldsymbol{\xi}_\alpha] \end{pmatrix}^{-1} \begin{pmatrix} \boldsymbol{\xi}_\alpha^{(1)} - \bar{\boldsymbol{\xi}}_\alpha^{(1)} \\ \boldsymbol{\xi}_\alpha^{(2)} - \bar{\boldsymbol{\xi}}_\alpha^{(2)} \\ \boldsymbol{\xi}_\alpha^{(3)} - \bar{\boldsymbol{\xi}}_\alpha^{(3)} \end{pmatrix} \right), \tag{17}$$

subject to the constraint that the true values $\bar{\boldsymbol{\xi}}_\alpha^{(k)}$ satisfy (6). Introducing Lagrange multipliers $\lambda_\alpha^{(k)}$ to (6), differentiating $J - \sum_{\alpha=1}^{N}\sum_{k=1}^{3}\lambda_\alpha^{(k)}(\bar{\boldsymbol{\xi}}_\alpha^{(k)}, \mathbf{u})$ with respect to $\bar{\boldsymbol{\xi}}_\alpha^{(1)}$, $\bar{\boldsymbol{\xi}}_\alpha^{(2)}$, and $\bar{\boldsymbol{\xi}}_\alpha^{(3)}$, and letting the result be $\mathbf{0}$, we obtain

$$-\begin{pmatrix} V_0^{(11)}[\boldsymbol{\xi}_\alpha] & V_0^{(12)}[\boldsymbol{\xi}_\alpha] & V_0^{(13)}[\boldsymbol{\xi}_\alpha] \\ V_0^{(21)}[\boldsymbol{\xi}_\alpha] & V_0^{(22)}[\boldsymbol{\xi}_\alpha] & V_0^{(23)}[\boldsymbol{\xi}_\alpha] \\ V_0^{(31)}[\boldsymbol{\xi}_\alpha] & V_0^{(32)}[\boldsymbol{\xi}_\alpha] & V_0^{(33)}[\boldsymbol{\xi}_\alpha] \end{pmatrix}^{-1} \begin{pmatrix} \boldsymbol{\xi}_\alpha^{(1)} - \bar{\boldsymbol{\xi}}_\alpha^{(1)} \\ \boldsymbol{\xi}_\alpha^{(2)} - \bar{\boldsymbol{\xi}}_\alpha^{(2)} \\ \boldsymbol{\xi}_\alpha^{(3)} - \bar{\boldsymbol{\xi}}_\alpha^{(3)} \end{pmatrix} - \begin{pmatrix} \lambda_\alpha^{(1)}\mathbf{u} \\ \lambda_\alpha^{(2)}\mathbf{u} \\ \lambda_\alpha^{(3)}\mathbf{u} \end{pmatrix} = \mathbf{0}, \tag{18}$$

from which we obtain

$$\bar{\boldsymbol{\xi}}_\alpha^{(k)} = \boldsymbol{\xi}_\alpha^{(k)} + \sum_{l=1}^{3} \lambda_\alpha^{(l)} V_0^{(kl)}[\boldsymbol{\xi}_\alpha]\mathbf{u}. \tag{19}$$

Substituting this into $(\bar{\boldsymbol{\xi}}_\alpha^{(k)}, \mathbf{u}) = 0$, we obtain

$$\sum_{l=1}^{3} \lambda_\alpha^{(l)} (\mathbf{u}, V_0^{(kl)}[\boldsymbol{\xi}_\alpha]\mathbf{u}) = -(\boldsymbol{\xi}_\alpha^{(k)}, \mathbf{u}), \tag{20}$$

which defines a set of linear equations in $\lambda_\alpha^{(k)}$. Let $\mathbf{V}_\alpha$ be the matrix whose (kl) element is $(\mathbf{u}, V_0^{(kl)}[\boldsymbol{\xi}_\alpha]\mathbf{u})$:

$$\mathbf{V}_\alpha = \big((\mathbf{u}, V_0^{(kl)}[\boldsymbol{\xi}_\alpha]\mathbf{u})\big). \tag{21}$$

The solution of (20) is written as

$$\lambda_\alpha^{(k)} = -\sum_{l=1}^{3} W_\alpha^{(kl)} (\boldsymbol{\xi}_\alpha^{(l)}, \mathbf{u}), \tag{22}$$

where $W_\alpha^{(kl)}$ is the (kl) element of $\mathbf{V}_\alpha^{-1}$, which we symbolically write as

$$W_\alpha^{(kl)} = \big((\mathbf{u}, V_0^{(kl)}[\boldsymbol{\xi}_\alpha]\mathbf{u})\big)^{-1}. \tag{23}$$

If (22) is substituted into (19), which is then substituted into (17), we can express the residual J in the form

$$J = \sum_{\alpha=1}^{N}\sum_{k,l=1}^{3} W_\alpha^{(kl)} (\boldsymbol{\xi}_\alpha^{(k)}, \mathbf{u})(\boldsymbol{\xi}_\alpha^{(l)}, \mathbf{u}), \tag{24}$$

which is to be minimized over the domain $\mathcal{U}$ of $\mathbf{u}$.

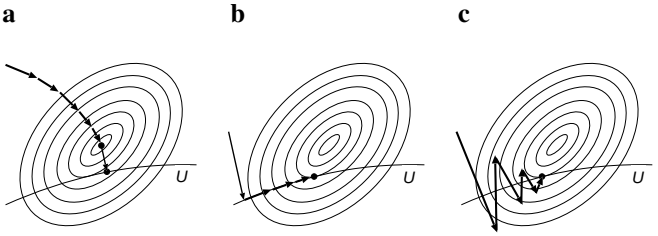

Figure 1: The solution is constrained to be in $\mathcal{U}$. (a) A posteriori correction. (b) Internal access. (c) External access.

4. Optimization with internal constraints

The strategies for minimizing a cost function J with internal constraints are roughly classified into three categories:

1. *A posteriori correction.* The function J is first minimized without considering the internal constraints and the solution $\mathbf{u}$ is modified *a posteriori* so as to satisfy them (Fig. 1(a)). For example, if the matrix $\mathbf{A}$ is constrained to be a rotation, we first we compute it as a general 3×3 matrix and then correct it to enforce $\mathbf{A}\mathbf{A}^\top = \mathbf{I}$ and $\det\mathbf{A} = 1$. The well known technique for this is the use of the singular value decomposition [5].
2. *Internal access.* The unknown $\mathbf{u}$ is parameterized so that internal constraints are identically satisfied. For example, if the matrix $\mathbf{A}$ is constrained to be a rotation, we parameterize it in terms of Euler angles or quaternions [4]. Then, the function J

is optimized in the resulting ("internal") parameter space of a smaller dimension (Fig. 1(b)).

3. *External access.* We do iterations in the unconstrained ("external") parameter space in such a way that the solution automatically satisfies the internal constraints at the time of convergence (Fig. 1(c)).

The EFNS of Kanatani and Sugaya [15] is an external access approach for computing the fundamental matrix $\mathbf{F}$ with the internal constraint $\det\mathbf{F} = 0$. However, it can deal with only a single scalar external constraint. We now extend it to multiple external constraints. Differentiating (24) with respect to $\mathbf{u}$, we obtain

$$\nabla_{\mathbf{u}} J = \sum_{\alpha=1}^{N}\sum_{k,l=1}^{3} \nabla_{\mathbf{u}} W_{\alpha}^{(kl)}(\boldsymbol{\xi}_{\alpha}^{(k)}, \mathbf{u})(\boldsymbol{\xi}_{\alpha}^{(l)}, \mathbf{u}) + 2\sum_{\alpha=1}^{N}\sum_{k,l=1}^{3} W_{\alpha}^{(kl)}(\boldsymbol{\xi}_{\alpha}^{(l)}, \mathbf{u})\boldsymbol{\xi}_{\alpha}^{(k)}. \tag{25}$$

Since $\mathbf{W} = (W_{\alpha}^{(kl)})$ is defined to be the inverse of the matrix $\mathbf{V}_{\alpha}$ in (21), we differentiate $\mathbf{V}_{\alpha}\mathbf{W}_{\alpha} = \mathbf{I}$ with respect to u_i on both sides to compute $\nabla_{\mathbf{u}} W_{\alpha}^{(kl)}$. From

$$\frac{\partial \mathbf{V}_{\alpha}}{\partial u_i}\mathbf{W}_{\alpha} + \mathbf{V}_{\alpha}\frac{\partial \mathbf{W}_{\alpha}}{\partial u_i} = \mathbf{O}, \tag{26}$$

we obtain

$$\frac{\partial \mathbf{W}_{\alpha}}{\partial u_i} = -\mathbf{V}_{\alpha}^{-1}\frac{\partial \mathbf{V}_{\alpha}}{\partial u_i}\mathbf{W}_{\alpha} = -\mathbf{W}_{\alpha}\frac{\partial \mathbf{V}_{\alpha}}{\partial u_i}\mathbf{W}_{\alpha}. \tag{27}$$

From (21), the (kl) element of the above equation is

$$\begin{aligned}\nabla_{\mathbf{u}} W_{\alpha}^{(kl)} &= -\sum_{m,n=1}^{3} W_{\alpha}^{(km)}\nabla_{\mathbf{u}}(\mathbf{u}, V_0^{(mn)}[\boldsymbol{\xi}_{\alpha}]\mathbf{u})W_{\alpha}^{(nl)} \\ &= -2\sum_{m,n=1}^{3} W_{\alpha}^{(km)}W_{\alpha}^{(nl)}V_0^{(mn)}[\boldsymbol{\xi}_{\alpha}]\mathbf{u}.\end{aligned} \tag{28}$$

After this is substituted, (25) becomes

$$\nabla_{\mathbf{u}} J = 2\Big(\sum_{\alpha=1}^{N}\sum_{k,l=1}^{3} W_{\alpha}^{(kl)}\boldsymbol{\xi}_{\alpha}^{(k)}\boldsymbol{\xi}_{\alpha}^{(l)\top}\Big)\mathbf{u} - 2\Big(\sum_{\alpha=1}^{N}\sum_{m,n=1}^{3} v_{\alpha}^{(m)}v_{\alpha}^{(n)}V_0^{(mn)}[\boldsymbol{\xi}_{\alpha}]\Big)\mathbf{u}, \tag{29}$$

where we define $v_{\alpha}^{(k)}$ by

$$v_{\alpha}^{(k)} = \sum_{l=1}^{3} W_{\alpha}^{(kl)}(\boldsymbol{\xi}_{\alpha}^{(l)}, \mathbf{u}). \tag{30}$$

Hence, if we define matrices $\mathbf{M}$ and $\mathbf{L}$ by

$$\mathbf{M} = \sum_{\alpha=1}^{N}\sum_{k,l=1}^{3} W_{\alpha}^{(kl)}\boldsymbol{\xi}_{\alpha}^{(k)}\boldsymbol{\xi}_{\alpha}^{(l)\top}, \qquad \mathbf{L} = \sum_{\alpha=1}^{N}\sum_{k,l=1}^{3} v_{\alpha}^{(k)}v_{\alpha}^{(l)}V_0^{(kl)}[\boldsymbol{\xi}_{\alpha}], \tag{31}$$

we can write (29) as

$$\nabla_{\mathbf{u}} J = 2(\mathbf{M} - \mathbf{L})\mathbf{u}. \tag{32}$$

As is well known in calculus, the residual J takes a stationary value at $\mathbf{u} \in \mathcal{U}$ if and only if the gradient $\nabla_{\mathbf{u}} J$ is orthogonal to $\mathcal{U}$ at $\mathbf{u}$; otherwise, we can move within $\mathcal{U}$ so that J increases/decreases. In terms of the space $\mathcal{N}_{\mathbf{u}}$ in (10), this stationarity condition is written as $\nabla_{\mathbf{u}} J \in \mathcal{N}_{\mathbf{u}}$. However, we can easily see that (24) is homogeneous in $\mathbf{u}$ with degree 0: the value J is unchanged if $\mathbf{u}$ is multiplied by any nonzero constant. Hence, $\nabla_{\mathbf{u}} J$ is everywhere orthogonal to $\mathbf{u}$. It follows from (12) that $\nabla_{\mathbf{u}} J \in \mathcal{N}_{\mathbf{u}}$ is equivalent to

$$\nabla_{\mathbf{u}} J \in \mathcal{M}_{\mathbf{u}}. \tag{33}$$

Let $\mathbf{P}_{\mathcal{M}}$ be the projection matrix onto the orthogonal complement $\mathcal{M}_{\mathbf{u}}^{\perp}$ of $\mathcal{M}_{\mathbf{u}}$. Then, (33) is equivalent to

$$\mathbf{P}_{\mathcal{M}}\nabla_{\mathbf{u}} J = \mathbf{0}. \tag{34}$$

From (13), we can see that $\mathbf{u}$ belongs to the domain $\mathcal{U}$ if and only if

$$\mathbf{P}_{\mathcal{M}}\mathbf{u} = \mathbf{u}. \tag{35}$$

Thus, the ML solution with internal constraints is obtained if we find a unit vector $\mathbf{u}$ that satisfies (34) and (35). We see that (32) and (34) imply

$$\mathbf{P}_{\mathcal{M}}(\mathbf{M} - \mathbf{L})\mathbf{u} = \mathbf{0}. \tag{36}$$

If (35) is satisfied, this can be written as

$$\mathbf{P}_{\mathcal{M}}(\mathbf{M} - \mathbf{L})\mathbf{P}_{\mathcal{M}}\mathbf{u} = \mathbf{0}. \tag{37}$$

Note that $\mathbf{P}_{\mathcal{M}}$ is a symmetric matrix. Thus, if we define the symmetric matrix

$$\mathbf{X} = \mathbf{P}_{\mathcal{M}}(\mathbf{M} - \mathbf{L})\mathbf{P}_{\mathcal{M}}, \tag{38}$$

finding the unit vector $\mathbf{u}$ that satisfies (34) and (35) is equivalent to finding the unit vector $\mathbf{u}$ that satisfies

$$\mathbf{X}\mathbf{u} = \mathbf{0}, \qquad \mathbf{P}_{\mathcal{M}}\mathbf{u} = \mathbf{u}. \tag{39}$$

The solution is obtained by the following iterations:

1. Provide an initial guess $\mathbf{u}$.
2. Compute the matrices $\mathbf{M}$ and $\mathbf{L}$ in (31).
3. Compute $\nabla_{\mathbf{u}}\phi_1(\mathbf{u})$, ..., $\nabla_{\mathbf{u}}\phi_r(\mathbf{u})$. Let $\{\mathbf{u}_1, ..., \mathbf{u}_r\}$ be the orthonormal system obtained from them by Schmidt orthogonalization, and compute the projection matrix
$$\mathbf{P}_{\mathcal{M}} = \mathbf{I} - \sum_{k=1}^{r}\mathbf{u}_k\mathbf{u}_k^{\top}, \tag{40}$$
where $\mathbf{I}$ here is the 13×13 identity matrix.
4. Compute the matrix $\mathbf{X}$ in (38).
5. Let $\mathbf{v}_0$, ..., $\mathbf{v}_r$ be the unit eigenvectors of $\mathbf{X}$ for the smallest $r+1$ eigenvalues.
6. Compute the projection $\hat{\mathbf{u}}$ of the current value $\mathbf{u}$ onto $\hat{\mathcal{N}}_{\mathbf{u}} = \{\mathbf{v}_0, ..., \mathbf{v}_r\}_{\mathcal{L}}$ as follows:
$$\hat{\mathbf{u}} = \sum_{k=0}^{r}(\mathbf{u}, \mathbf{v}_k)\mathbf{v}_k. \tag{41}$$
7. Compute
$$\mathbf{u}' = \mathcal{N}[\mathbf{P}_{\mathcal{M}}\hat{\mathbf{u}}], \tag{42}$$
where $\mathcal{N}[\cdot]$ denotes normalization to unit norm ($\mathcal{N}[\mathbf{a}] = \mathbf{a}/\|\mathbf{a}\|$).
8. If $\mathbf{u}' \approx \mathbf{u}$, return $\mathbf{u}'$ and stop. Else, let $\mathbf{u} \leftarrow \mathcal{N}[\mathbf{u} + \mathbf{u}']$, and go back to Step 2.

Justification. The proof that the above iterations produce the desired solution is as follows. We first show that at the time of convergence the space $\hat{\mathcal{N}}_{\mathbf{u}}$ computed in Step 4 coincides with the null space of $\mathbf{X}$. The definition of $\mathbf{P}_{\mathcal{M}}$ in (40) implies $\mathbf{P}_{\mathcal{M}}\mathbf{u}_k = \mathbf{0}$, $k = 1, ..., r$. From the definition of $\mathbf{X}$ in (38), this means that $\mathbf{u}_1$, ..., $\mathbf{u}_r$ are all null vectors of $\mathbf{X}$, i.e., eigenvectors with eigenvalue 0. Hence, the r of the $r+1$ vectors $\mathbf{v}_0$, ..., $\mathbf{v}_r$ computed in Step 5 are null vectors of $\mathbf{X}$. If $\hat{\mathcal{N}}_{\mathbf{u}}$ is not the null space of $\mathbf{X}$, one of $\mathbf{v}_0$, ..., $\mathbf{v}_r$, say $\mathbf{v}_*$ has a nonzero eigenvalue λ_* ($\neq 0$) and is orthogonal to the rest. Since the remaining r vectors span the space $\mathcal{M}_{\mathbf{u}} = \{\mathbf{u}_1, ..., \mathbf{u}_r\}_{\mathcal{L}}$, the vector $\mathbf{v}_*$ is orthogonal to $\mathcal{M}_{\mathbf{u}}$.

By construction, the vector $\hat{\mathbf{u}}$ of (41) is an element of $\hat{\mathcal{N}}_{\mathbf{u}} = \{\mathbf{v}_*\}_{\mathcal{L}} \oplus \mathcal{M}_{\mathbf{u}}$. Since $\mathbf{u}'$ of (42) is its orthogonal projection onto $\mathcal{M}_{\mathbf{u}}^{\perp}$ within $\hat{\mathcal{N}}_{\mathbf{u}}$, it equals $\pm\mathbf{v}_*$. At the time of the convergence of the iterations, $\mathbf{u} = \mathbf{u}' = \pm\mathbf{v}_*$ is satisfied. Since $\mathbf{v}_*$ is the eigenvector of $\mathbf{X}$ with eigenvalue λ_*, we have $\mathbf{X}\mathbf{u} = \lambda_*\mathbf{u}$ holds. Computing the inner product with $\mathbf{u}$ on both sides, we obtain

$$(\mathbf{u}, \mathbf{X}\mathbf{u}) = \lambda_* (\neq 0). \tag{43}$$

However, $\mathbf{u}$ ($=\pm\mathbf{v}_*$) is orthogonal to all the null vectors of $\mathbf{X}$, so it is orthogonal to the space $\mathcal{M}_\mathbf{u}$. Hence,

$$\mathbf{P}_\mathcal{M}\mathbf{u} = \mathbf{u}, \tag{44}$$

from which we see that

$$(\mathbf{u}, \mathbf{X}\mathbf{u}) = (\mathbf{u}, \mathbf{P}_\mathcal{M}(\mathbf{M}-\mathbf{L})\mathbf{P}_\mathcal{M}\mathbf{u}) = (\mathbf{u}, (\mathbf{M}-\mathbf{L})\mathbf{u}) = (\mathbf{u}, \mathbf{M}\mathbf{u})-(\mathbf{u}, \mathbf{L}\mathbf{u}). \tag{45}$$

On the other hand, we can show that $(\mathbf{u}, \mathbf{M}\mathbf{u}) = (\mathbf{u}, \mathbf{L}\mathbf{u})$ identically holds as follows:

$$\begin{aligned}
(\mathbf{u}, \mathbf{M}\mathbf{u}) &= \sum_{\alpha=1}^{N}\sum_{k,l=1}^{3} W_\alpha^{(kl)}(\boldsymbol{\xi}_\alpha^{(k)}, \mathbf{u})(\boldsymbol{\xi}_\alpha^{(l)}, \mathbf{u}),\\
(\mathbf{u}, \mathbf{L}\mathbf{u}) &= \sum_{\alpha=1}^{N}\sum_{k,l=1}^{3} v_\alpha^{(k)} v_\alpha^{(l)}(\mathbf{u}, V_0^{(kl)}[\boldsymbol{\xi}_\alpha]\mathbf{u})\\
&= \sum_{\alpha=1}^{N}\sum_{k,l=1}^{3}\Big(\sum_{m=1}^{3} W_\alpha^{(km)}(\boldsymbol{\xi}_\alpha^{(m)}, \mathbf{u})\Big)\Big(\sum_{n=1}^{3} W_\alpha^{(ln)}(\boldsymbol{\xi}_\alpha^{(n)}, \mathbf{u})\Big)V_\alpha^{(kl)}\\
&= \sum_{\alpha=1}^{N}\sum_{m,n=1}^{3}\Big(\sum_{k,l=1}^{3} W_\alpha^{(mk)} V_\alpha^{(kl)} W_\alpha^{(ln)}\Big)(\boldsymbol{\xi}_\alpha^{(m)}, \mathbf{u})(\boldsymbol{\xi}_\alpha^{(n)}, \mathbf{u})\\
&= \sum_{\alpha=1}^{N}\sum_{m,n=1}^{3} W_\alpha^{(mn)}(\boldsymbol{\xi}_\alpha^{(m)}, \mathbf{u})(\boldsymbol{\xi}_\alpha^{(n)}, \mathbf{u}).
\end{aligned} \tag{46}$$

Here, we have noted that $\mathbf{W}_\alpha = \mathbf{V}_\alpha^{-1}$ and hence $\mathbf{W}_\alpha\mathbf{V}_\alpha\mathbf{W}_\alpha = \mathbf{W}_\alpha$. Thus, we conclude that $(\mathbf{u}, \mathbf{X}\mathbf{u}) = 0$, which contradicts (43). This means that at the time of convergence, all elements of $\hat{\mathcal{N}}_\mathbf{u}$ are null vectors of $\mathbf{X}$. Since $\mathbf{u} = \mathbf{u}' = \pm\mathbf{v}_* \in \hat{\mathcal{N}}_\mathbf{u}$, we see that $\mathbf{X}\mathbf{u} = \mathbf{0}$. Considering (44), we see that $\mathbf{u}$ (a unit vector by construction) satisfies (39). □

In Step 5 of the procedure, it would seem more natural to compute the smallest $r+1$ eigenvalues in absolute value, but we have confirmed by experiments that convergence is faster for computing the smallest $r+1$ eigenvalue. The same was observed for the original FNS of Chojnacki et al. [2] and the EFNS of Kanatani and Sugaya [15], for which convergence is faster for computing the smallest eigenvalue rather than the smallest eigenvalue in absolute value [15, 14].

Theoretically, Step 8 of the procedure could be "if $\mathbf{u} \approx \mathbf{u}$, return $\mathbf{u}'$ and stop. Else, let $\mathbf{u} \leftarrow \mathbf{u}'$ and go back to Step 2". In order to improve convergence, however, the "midpoint" $(\mathbf{u}' + \mathbf{u})/2$ is normalized to a unit vector $\mathcal{N}[\mathbf{u}' + \mathbf{u}]$, which greatly improves convergence. In fact, we have confirmed that this technique also improves the convergence of the original FNS of Chojnacki et al. [2], which sometimes oscillates in the presence of large noise.

5. Motion interpretation experiment

Suppose a curved grid surface expands by s_x, s_y, and s_z in the x, y, and z directions, respectively, rotates around an axis passing through the origin by angle Ω, and translates by $\mathbf{t}$, as depicted in Fig. 2 (above). Here, we consider the following nine different motions:

0. affinity: $\Omega = 10°$, $\mathbf{t} = (100, 100, 300)^\top$, $s_x = 1.01$, $s_y = 1.02$, $s_z = 0.99$.
1. similarity: $\Omega = 10°$, $\mathbf{t} = (100, 100, 300)^\top$, $s_x = s_y = s_z = 1.01$.
2. rigid motion: $\Omega = 10°$, $\mathbf{t} = (100, 100, 300)^\top$, $s_x = s_y = s_z = 1$.
3. rotation and scale change: $\Omega = 10°$, $\mathbf{t} = \mathbf{0}$, $s_x = s_y = s_z = 1.01$.
4. translation and scale change: $\Omega = 0$, $\mathbf{t} = (100, 100, 300)^\top$, $s_x = s_y = s_z = 1.01$.
5. rotation: $\Omega = 10°$, $\mathbf{t} = \mathbf{0}$, $s_x = s_y = s_z = 1$.
6. translation: $\Omega = 0$, $\mathbf{t} = (100, 100, 300)^\top$, $s_x = s_y = s_z = 1$.
7. scale change: $\Omega = 0$, $\mathbf{t} = \mathbf{0}$, $s_x = s_y = s_z = 1.01$.
8. identity: $\Omega = 0$, $\mathbf{t} = \mathbf{0}$, $s_x = s_y = s_z = 1$.

We measure the 3-D positions of the grid points by stereo vision before and after each motion. The center of the grid surface is at the coordinate origin O before the motion, and the two cameras are positioned so that the disparity angle of the origin O is 10°. The simulated stereo images for the motion 0 are shown in Fig. 2 (below). The image size is set to 500×800 pixels and the focal length to 600 pixels. We added independent Gaussian noise of mean 0 and standard deviation σ pixels to the x and y coordinates of the grid points in the images and reconstructed their 3-D positions $\hat{\mathbf{r}}_\alpha$ and $\hat{\mathbf{r}}'_\alpha$ by the method of Kanatani et al. [16]. Although the noise in 2-D is homogeneous and isotropic, the induced noise in 3-D is inhomogeneous and anisotropic; an uncertainty ellipsoid is illustrated in Fig. 2 (above). The normalized covariance matrices $V_0[\hat{\mathbf{r}}_\alpha]$ and $V_0[\hat{\mathbf{r}}'_\alpha]$ of the reconstructed points $\hat{\mathbf{r}}_\alpha$ and $\hat{\mathbf{r}}'_\alpha$ can be evaluated by the method of Kanatani and Niitsuma [13]. To the thus generated $\hat{\mathbf{r}}_\alpha$ and $\hat{\mathbf{r}}'_\alpha$, we fitted the following nine models:

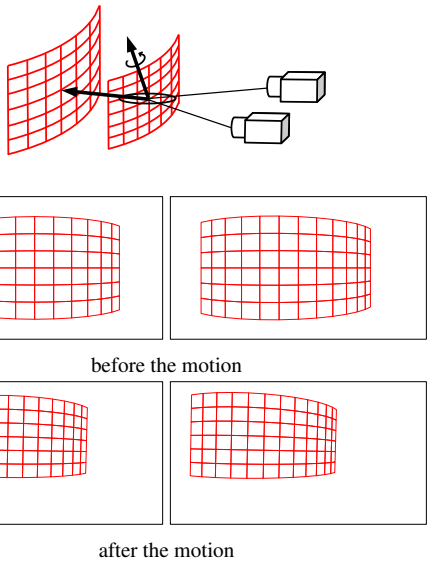

Figure 2: Above: Stereo vision of a grid surface that undergoes a similarity (rotation, translation, and scale change). An uncertainty ellipsoid is illustrated. Below: Simulated stereo image pairs before and after the motion (the motion 0).

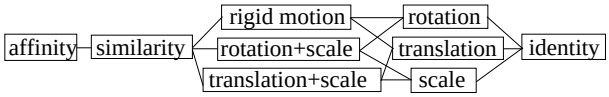

Figure 3: The inclusion relationships of the subgroups of the 3-D affinity.

0. affinity: no internal constraints.
1. similarity: $\phi_1(\mathbf{u})$, ..., $\phi_5(\mathbf{u})$.
2. rigid motion: $\phi_1(\mathbf{u})$, ..., $\phi_6(\mathbf{u})$.
3. rotation and scale change: $\phi_1(\mathbf{u})$, ..., $\phi_5(\mathbf{u})$, $\phi_{16}(\mathbf{u})$, $\phi_{17}(\mathbf{u})$, $\phi_{18}(\mathbf{u})$.
4. translation and scale change: $\phi_7(\mathbf{u})$, ..., $\phi_{14}(\mathbf{u})$.
5. rotation: $\phi_1(\mathbf{u})$, ..., $\phi_6(\mathbf{u})$, $\phi_{16}(\mathbf{u})$, $\phi_{17}(\mathbf{u})$, $\phi_{18}(\mathbf{u})$.
6. translation: $\phi_7(\mathbf{u})$, ..., $\phi_{15}(\mathbf{u})$.
7. scale change: $\phi_7(\mathbf{u})$, ..., $\phi_{14}(\mathbf{u})$, $\phi_{16}(\mathbf{u})$, $\phi_{17}(\mathbf{u})$, $\phi_{18}(\mathbf{u})$.
8. identity: $\phi_7(\mathbf{u})$, ..., $\phi_{18}(\mathbf{u})$.

The inclusion relationships among these models is shown in Fig. 3. We fitted each of the nine models to all the nine motions by our EFNS procedure. We found that a good initial guess is required to ensure convergence of the EFNS iterations. This becomes more crucial as the number of imposed constraints increases. For this, we used the well known least squares procedure [13], which we found to be sufficient to ensure convergence. To be specific, the translation $\mathbf{t}$ is estimated from the displacement of the centroid of the N points before and after the motion, the scale change s (assuming that $s_x = s_y = s_z$) is estimated from the change of the RMS

distance of the points from their centroid, and the rotation **R** is estimated by using SVD [5]. Then, they are adjusted appropriately: **R** is replaced by **I** if rotation is not included; **t** is replace by **0** if translation is not included; s is replaced by 1 if scale change is not included. We let the reference length to be $L_0 = 1000$. The EFNS converged after around 10 iterations for a moderate number of constraints and around 20 iterations for a large number of constraints.

We also compared our method with the standard procedure: we introduced model-specific parameters such as quaternions and minimized the residual by the Levenberg-Marquardt method [23]. We confirmed that the same solution as our EFNS procedure is obtained. The Levenberg-Marquardt method is unconstrained optimization in the parameter space, and its convergence depends on the particular parameterization used and the initial solution to start, but it usually converges smoothly over a relatively large domain of the initial solution. The advantage of our EFNS method is that we need no particular parameterization for particular modes. On the other hand, it has the disadvantage that we need a good initial guess and that convergence may take time depending on the number of constraints.

Then, we did motion inference experiment, inferring the true motion from observed noisy motion and the residual of each of the fitted models, using the geometric AIC [9], the geometric BIC [12], and the geometric MDL [11], which has the same form as the geometric BIC (their meanings are given shortly). They are given by

$$\text{G-AIC} = \hat{J} + 2(3N + p)\sigma^2,$$
$$\text{G-BIC} = \text{G-MDL} = \hat{J} - (3N + p)\sigma^2 \log \frac{\sigma^2}{L_0^2}. \tag{47}$$

The model which has the smallest value of these are chosen as most likely. Here, $\hat{J}$ is the residual J of the fit, N is the number of points (91 grid points in this experiment), and p is the degree of freedom of the model: for the above models 0, 1, ..., 8, it is $p = 12, 7, 6, 4, 4, 3, 3, 1, 0$, respectively. Since all the models are subgroups of the 3-D affinity (Fig. 3), the noise level σ is estimated from the residual J_0 of the most general model 0 in the following form [5]:

$$\hat{\sigma}^2 = \frac{\hat{J}_0}{3N - 12}. \tag{48}$$

Table 1 lists for each of the nine motions (columns) the percentage of each of the nine models (rows) being chosen by the geometric AIC and the geometric BIC/MDL after independent 100 trials, each time using different noise of $\sigma = 1$. We can see that although the correct model is not always chosen, the correct choice is made with a large probability. We can also see that the geometric BIC/MDL can make better choice for motions with small degrees of freedom. However, they tends to choose simpler models for motions with large degrees of freedom. For example, even though the true model is 3 (rotation and scale change), the simpler model 5 (rotation) is more frequently chosen, meaning that the effect (i.e., the residual change) of scale is not large enough to affect the judgment. This is because the penalty for the model complexity is heavier for the geometric BIC/MDL than the geometric AIC. It is widely known that the use of the geometric BIC/MDL has the advantage that the judgement is robust to insignificant disturbances, while the geometric AIC is more faithful to the observation. The actual values of the G-AIC, the G-BIC (= G-MDL) for a particular noise case are listed in Table 2; the chosen models are indicated by underlines. We can see that the differences from the second best models are very small when the true motion is not chosen.

Table 1:
The percentage of each model being chosen by the geometric AIC and the geometric BIC/MDL.

Motion	0	1	2	3	4	5	6	7	8
Geometric AIC									
model 0	100	3	6	6	3	1	3	3	0
model 1	0	97	17	5	9	2	1	2	2
model 2	0	0	77	0	2	10	6	0	3
model 3	0	0	0	89	0	16	0	11	1
model 4	0	0	0	0	85	0	19	7	0
model 5	0	0	0	0	0	71	0	0	4
model 6	0	0	0	0	1	0	71	0	7
model 7	0	0	0	0	0	0	0	77	5
model 8	0	0	0	0	0	0	0	0	78
Geometric BIC/MDL									
model 0	39	0	0	0	0	0	0	0	0
model 1	61	46	0	0	0	0	0	0	0
model 2	0	54	100	0	0	0	0	0	0
model 3	0	0	0	86	0	0	0	0	0
model 4	0	0	0	0	33	0	0	0	0
model 5	0	0	0	14	0	100	0	0	0
model 6	0	0	0	0	67	0	100	0	0
model 7	0	0	0	0	0	0	0	100	0
model 8	0	0	0	0	0	0	0	0	100

Table 2: The values of the G-AIC and the G-BIC (= G-MDL) for a particular noise case ($\times 10^2$). The underlines indicate the chosen models.

motion	0	1	2	3	4	5	6	7	8
G-AIC									
model 0	6.9751	8.1379	8.6326	7.6066	9.1490	9.8183	6.9272	8.2901	7.5678
model 1	7.6925	8.1394	8.5269	7.5305	9.0370	9.7532	6.8708	8.2307	7.5128
model 2	8.2663	8.2013	8.5476	7.6065	9.2824	9.7294	6.9200	8.4536	7.4958
model 3	1204.5	1359.6	1380.3	7.4832	1407.2	9.6857	1430.5	8.1803	7.4871
model 4	143.71	141.51	137.43	130.09	9.0017	133.52	6.8647	8.1820	7.4871
model 5	1188.0	1341.4	1363.9	7.5588	1339.4	9.6620	1369.9	8.4298	7.4691
model 6	142.83	140.47	136.83	129.72	9.2480	133.13	6.9112	8.4054	7.4701
model 7	2572.9	2609.8	2632.0	1970.5	2099.5	1978.4	2140.5	8.1383	7.4544
model 8	3014.9	2943.4	2950.6	5207.0	2319.3	5230.9	2371.7	8.5386	7.4362
G-BIC/G-MDL									
model 0	35.659	41.173	43.501	38.661	45.921	49.043	35.430	41.890	38.477
model 1	35.873	40.595	42.784	38.040	45.164	48.290	34.874	41.242	37.880
model 2	36.346	40.541	42.682	38.007	45.280	48.128	34.823	41.347	37.754
model 3	1232.4	1391.8	1414.2	37.666	1442.9	47.809	1458.2	40.837	37.529
model 4	171.59	173.62	171.32	160.27	44.742	171.65	34.568	40.839	37.529
model 5	1215.8	1373.3	1397.6	37.633	1375.0	47.648	1397.5	40.969	37.402
model 6	170.61	172.46	170.60	159.79	44.859	171.11	34.514	40.945	37.403
model 7	2600.5	2641.6	2665.5	2000.3	2134.9	2016.1	2167.9	40.442	37.171
model 8	3042.4	2975.0	2984.0	5236.7	2354.6	5268.4	2399.0	40.724	37.044

The geometric AIC is based on Akaike's *AIC* (*Akaike Information Criterion*) [1]. It is derived from the Kullback-Leibler distance combined with bias correction. Akaike's AIC is obtained by asymptotic approximation for $N \to \infty$ with a large number N of observations, while the geometric AIC is obtained by perturbation expansion for $\sigma \to 0$ with a small noise level σ [9]. The geometric BIC is based on Schwarz' *BIC* (*Bayesian Information Criterion*) [25]. It is derived from the a posteriori probability combined with Laplace expansion. Schwarz's BIC is obtained by asymptotic approximation for $N \to \infty$ with a large number N of observations, while the geometric BIC is obtained by perturbation expansion for $\sigma \to 0$ with a small noise level σ [12]. The geometric MDL is based on Rissanen's *MDL* (*Minimum Description Length*) [24]. It is derived from the minimum description length of the problem and the data combined with optimal quantization of real numbers. Rissanen's MDL is obtained by asymptotic approximation for $N \to \infty$ with a large number N of observations, while the geometric MDL is obtained by perturbation expansion for $\sigma \to 0$ with a small noise level σ [11].

Geometric model selection using the geometric AIC and the geometric BIC/MDL have been done for many problems of computer vision, including fitting lines, curves, planes, and surfaces to 2-D and 3-D points [11], reliability evaluation of 3-D computation using a moving camera [7], detecting symmetry of 2-D shapes [6], segmenting a curve into line segments [8], inferring object shapes by stereo vision [17], moving object detection from optical flow [22], camera motion estimation for virtual studio systems [20], correspondence detection between images [19], automatic regularity enforcement on 2-D figures [27], automatic image mosaicing [18], and multibody motion segmentation [10, 26]. From these experiences, it has been recognized that the geometric AIC has a tendency to favor a model that has a smaller residual if the degree of freedom of the model is not so different, while the geometric BIC/MDL has a tendency to favor a model with a smaller degree of freedom if the residual is not so different. We can also observe these tendencies from our experiment.

6. Real GPS geodesic data analysis

Geodetic scientists all over the world monitor the land deformation using GPS data. Table 3 shows the x, y, and z coordinates (in meters) with respect to the global earth coordinate system, called WGS84 (World Geodetic System 1984), of eight positions in northeast Japan (Fig. 4) in January 2010, April 2011, and April 2012 provided by the Geospatial Information Authority of Japan[1]. The location IDs 0036, 0172, 0175, 0549, 0550, 0914, 0916, and 0918 in Table 3 correspond to Onagawa, Kesennuma, Shizugawa, Yamoto, Oshika, Towa, Minamikata, and Kahoku, respectively, as indicated in Fig. 4. The covariance matrices

$$\begin{pmatrix} \sigma_{11} & \sigma_{12} & \sigma_{13} \\ \sigma_{12} & \sigma_{22} & \sigma_{23} \\ \sigma_{13} & \sigma_{23} & \sigma_{33} \end{pmatrix}$$

of each measurement are listed in Table 4. We regarded $(-3899900, 3116600, 3956400)$ as a tentative coordinate origin and used the reference length $L_0 = 1000$. The optimally fitted affinity of the land between April 2010 and January 2011 is

$$\begin{pmatrix} x' \\ y' \\ z' \end{pmatrix} = \begin{pmatrix} 0.999971299834119 & 0.000022846760455 \\ 0.000032692122035 & 0.999974183470998 \\ -0.000010763169341 & 0.000008714718681 \end{pmatrix}$$

[1] http://www.gsi.go.jp/

Table 3:
The 3-D data (in meters) of eight locations in northeast Japan in April 2010, January 2011, and January 2012.

ID	x	y	z
April 2010			
0036	−3911124.6109	3117611.8596	3944663.0892
0172	−3893613.1472	3089073.9138	3983982.4425
0175	−3898936.7310	3106983.5744	3964933.7807
0549	−3899954.0638	3134197.0846	3942545.9721
0550	−3922366.9569	3119914.9630	3931806.3441
0914	−3888499.5166	3113285.6200	3970160.1127
0916	−3884406.9622	3127530.4255	3963000.4271
0918	−3900409.6500	3124326.0455	3949941.0937
January 2011			
0036	−3911124.6161	3117611.8674	3944663.0891
0172	−3893613.1407	3089073.9247	3983982.4331
0175	−3898936.7224	3106983.5798	3964933.7745
0549	−3899954.0672	3134197.0985	3942545.9686
0550	−3922366.9488	3119914.9518	3931806.3269
0914	−3888499.5075	3113285.6240	3970160.1054
0916	−3884406.9628	3127530.4296	3963000.4215
0918	−3900409.6423	3124326.0532	3949941.0840
January 2012			
0036	−3911128.3589	3117608.0272	3944661.2547
0172	−3893616.5621	3089070.9017	3983980.4920
0175	−3898940.3307	3106980.2371	3964931.9731
0549	−3899957.3856	3134193.9276	3942544.6596
0550	−3922370.7681	3119910.6783	3931804.3063
0914	−3888502.8233	3113282.7641	3970158.5816
0916	−3884410.1104	3127527.7274	3962999.1209
0918	−3900413.1310	3124322.7276	3949939.5679

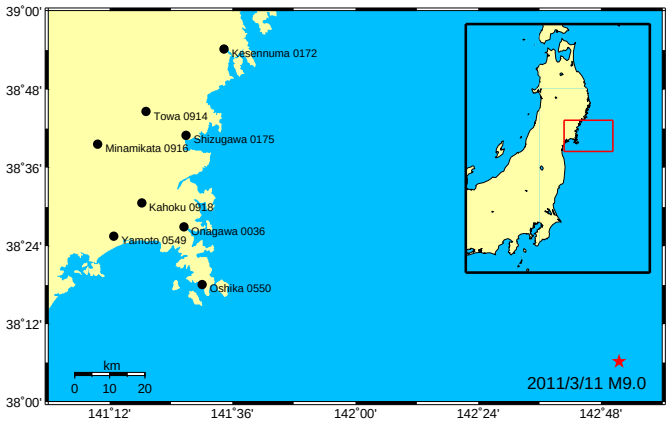

Figure 4: Eight locations (black circles) in northeast Japan and the epicenter (the star mark) of the earthquake on 11 March 2011.

$$\begin{pmatrix} 0.000029511830098 \\ -0.000033202523519 \\ 1.000011020834165 \end{pmatrix} \begin{pmatrix} x \\ y \\ z \end{pmatrix} + \begin{pmatrix} -299.8902360559441 \\ 339.3263535494916 \\ -112.7441873988137 \end{pmatrix} \tag{49}$$

with respect to the original coordinate system. Although in theory any nonlinear deformation can be possible, yearly land deformation is usually so small that affinity is regarded as the most general motion for geodetic analysis.

Figure 5(a) shows the land movement (1000 times magnified) after converting the global earth coordinates to the local

Table 4: Covariance matrices ($\times 10^{-8}$) of the GPS measurements in Table 3.

ID	0036	0172	0175	0549	0550	0914	0916	0918
April 2010								
σ_{11}	543.81468	2600.5301	588.95526	299.42994	2298.3728	2580.3350	510.26601	2230.8269
σ_{22}	425.88304	2395.0165	557.68621	206.77237	2204.4857	2378.9566	473.90957	2148.0015
σ_{33}	320.91074	1180.6302	306.88459	187.97368	970.31985	1113.2217	255.43911	958.60970
σ_{23}	204.01142	655.80839	222.80817	129.75187	555.38549	609.86213	181.32306	530.02453
σ_{31}	−262.01505	−765.87092	−252.43021	−173.89883	−658.16237	−830.68293	−225.06877	−625.30146
σ_{12}	−143.09649	−145.37253	−155.31865	−117.32354	−141.02400	−180.97003	−143.14545	−98.325922
January 2011								
σ_{11}	287.87533	249.12117	452.82105	247.77608	2300.5173	2509.0785	1664.8206	803.41570
σ_{22}	208.37832	192.85786	371.08918	189.61635	1811.4054	1958.3768	1707.0988	592.74803
σ_{33}	186.80209	161.45344	230.58634	154.45629	869.80636	978.14059	822.11796	316.10716
σ_{23}	125.56468	110.72924	143.89346	106.81192	412.96236	417.99055	400.88891	182.73249
σ_{31}	−170.69383	−143.73564	−198.90161	−139.79921	−627.57330	−766.42047	−523.79020	−261.03986
σ_{12}	−112.37926	−93.520583	−101.24319	−90.106188	−71.178480	−71.479138	−43.792427	−84.101060
January 2012								
σ_{11}	305.96250	250.29374	384.59613	250.86478	273.56924	2514.4584	586.20375	274.97742
σ_{22}	215.96414	191.07272	222.83353	182.75383	195.10014	1960.5877	568.93574	178.45872
σ_{33}	212.30943	161.34809	219.11424	157.11409	162.31885	1000.0640	300.81322	156.79702
σ_{23}	135.52470	108.43137	141.58703	103.04156	111.27658	42.292048	179.18146	101.31024
σ_{31}	−190.15388	−145.39350	−211.37678	−141.09274	−154.20913	−771.60432	−299.18962	−140.78606
σ_{12}	−122.02639	−97.485117	−130.11266	−91.186199	−103.82372	−58.595343	−101.51431	−89.699310

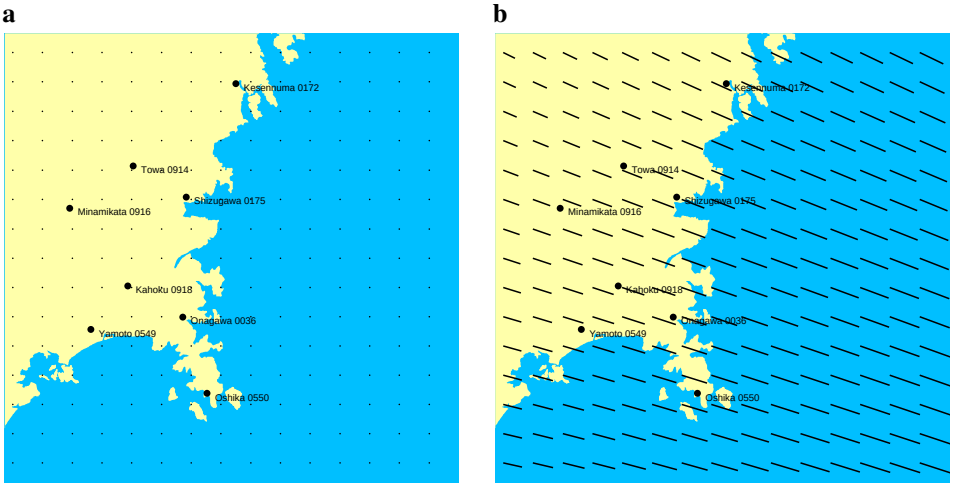

Figure 5: Land movement magnified 1000 times. (a) Between April 2010 and January 2011. (b) Between January 2011 and January 2012. The land appears to move uniformly south east toward the epicenter (the star mark in Fig. 4).

coordinates. For this display, we used the GMT (Generic Mapping Tools) [2]provided by the University of Hawaii at Manoa. This affine transformation makes the residual the smallest: if we fit a subgroup, e.g., a rigid motion, the residual necessarily increases, since subgroups have smaller degrees of freedom. The use of the geometric AIC and the geometric BIC/MDL balances this residual increase and the model degree of model freedom. The computed residual J, G-AIC, and G-BIC (= G-MDL) are listed in Table 5; the chosen models are indicated by underlines. As we see, the geometric AIC judges that only a translation took place, although the residual is very large. However, the geometric BIC/MDL, preferring simpler models, judges that the land did not move at all, even though the residual of identity is far larger than any other motion models. So, we conclude that the land was very stable in this period and that a minute translation may have took place if anything.

[2] `http://gmt.soest.hawaii.edu/`

The affine transformation that best fits the data in January 2011 and January 2012 is

$$\begin{pmatrix} x' \\ y' \\ z' \end{pmatrix} = \begin{pmatrix} 1.001228379683353 & -0.000959897405742 & -0.001235998473807 \\ 0.000950467968687 & 0.999279166869626 & -0.000926414154749 \\ 0.000338476069078 & -0.000240252011947 & 0.999671735382466 \end{pmatrix} \begin{pmatrix} x \\ y \\ z \end{pmatrix} + \begin{pmatrix} 12668.80530537805 \\ 9615.24810701143 \\ 3365.90110431844 \end{pmatrix}. \tag{50}$$

Figure 5(b) shows the corresponding movement (1000 times magnified). The computed residual J, G-AIC, and G-BIC (= G-MDL) are listed in Table 6; the chosen models are indicated by underlines. The deformation shown in Fig. 5(b) appears to be a uniform translation toward the epicenter (the star mark in Fig. 4), but the geometric AIC and the geometric BIC/BIC both choose the

Table 5:
The residual J, G-AIC, and G-BIC (= G-MDL) of each model for the deformation between April 2010 and January 2011. The models chosen by these criteria are indicated by underlines.

Model	J	G-AIC	G-BIC/MDL
0	2.7003×10^{-7}	1.8902×10^{-6}	2.5727×10^{-5}
1	3.4728×10^{-7}	1.7424×10^{-6}	2.2269×10^{-5}
2	3.7689×10^{-7}	1.7270×10^{-6}	2.1591×10^{-5}
3	1.8191×10^{-6}	3.0792×10^{-6}	2.1619×10^{-5}
4	4.6868×10^{-7}	1.7288×10^{-6}	2.0269×10^{-5}
5	2.3356×10^{-6}	3.5507×10^{-6}	2.1429×10^{-5}
6	5.0286×10^{-7}	$\underline{1.7180 \times 10^{-6}}$	1.9596×10^{-5}
7	1.9123×10^{-6}	3.0374×10^{-6}	1.9591×10^{-5}
8	2.4397×10^{-6}	3.5198×10^{-6}	$\underline{1.9411 \times 10^{-5}}$

Table 6:
The residual J, G-AIC, and G-BIC (= G-MDL) of each model for the deformation between January 2011 and January 2012. The models chosen by these criteria are indicated by underlines.

Model	J	G-AIC	G-BIC/MDL
0	4.3727×10^{-5}	$\underline{3.0609 \times 10^{-4}}$	$\underline{3.4988 \times 10^{-3}}$
1	3.6948×10^{-3}	3.9207×10^{-3}	6.6700×10^{-3}
2	4.5971×10^{-3}	4.8157×10^{-3}	7.4762×10^{-3}
3	5.3537×10^{-1}	5.3557×10^{-1}	5.3805×10^{-1}
4	4.4057×10^{-3}	4.6098×10^{-3}	7.0930×10^{-3}
5	5.3544×10^{-1}	5.3564×10^{-1}	5.3816×10^{-1}
6	5.4640×10^{-3}	5.6608×10^{-3}	8.0553×10^{-3}
7	5.4541×10^{-1}	5.4559×10^{-1}	5.4781×10^{-1}
8	5.4563×10^{-1}	5.4581×10^{-1}	5.4794×10^{-1}

affinity: They judge that the deformation cannot be explained by any of its subgroups. This reflects the very fact that a massive earthquake of magnitude 9.0 took place on 11 March 2011 in this region.

7. Concluding remarks

We proposed a new computational technique for fitting different motion models to noisy 3-D sensor data in a *unified* framework; no particular parameterization is required to particular motion models. Our method is obtained by generalizing the EFNS of Kanatani and Sugaya [15] to 3-D motion models with the observation that subgroups of 3-D affinity are defined by various internal constraints on the parameters. We applied our method to simulated stereo vision data for motion interpretation, using the geometric AIC and the geometric BIC/MDL. We also applied our method to the GPS geodetic data of the land deformation in northeast Japan, where a massive earthquake took of magnitude 9.0 place on 11 March 2011. It is expected that our EFNS technique will be widely used for 3-D analysis involving hierarchical motion models in various domains including computer vision, robotic navigation, and geodetic science.

Acknowledgments

The authors thank Orhan Akyilmaz of Istanbul Institute of Technology, Turkey, for helpful discussions about geodetic analysis. They also thank Takuto Honda of Hitachi Systems, Ltd., Japan, for helping our numerical experiments. This work was supported in part by JSPS Grant-in-Aid for Challenging Exploratory Research (24650086).

References

[1] H. Akaike, A new look at the statistical model identification, IEEE Transactions on Automatic Control 26 (1974) 716–723.
[2] W. Chojnacki, M.J. Brooks, A. van den Hengel, D. Gawley, On the fitting of surfaces to data with covariances, IEEE Transactions on Pattern Analysis and Machine Intelligence 22 (2000) 1294–1303.
[3] R. Hartley, A. Zisserman, Multiple View Geometry in Computer Vision, 2nd ed., Cambridge University Press, Cambridge, 2004.
[4] K. Kanatani, Group-Theoretical Methods in Image Understanding, Springer-Verlag, Berlin, 1990.
[5] K. Kanatani, Statistical Optimization for Geometric Computation: Theory and Practice, Elsevier Science, Amsterdam, 1996; reprinted, Dover, New York, 2005.
[6] K. Kanatani, Comments on 'Symmetry as a Continuous Feature', IEEE Transactions on Pattern Analysis and Machine Intelligence 19 (1997) 246–247.
[7] K. Kanatani, Self-evaluation for active vision by the geometric information criterion, in: Proceedings of the Seventh International Conference on Computer Analysis of Images and Patterns, 1997, pp. 247–254.
[8] K. Kanatani, Comments on 'Nonparametric Segmentation of Curves into Various Representations', IEEE Transactions on Pattern Analysis and Machine Intelligence 19 (1997) 1391–1392.
[9] K. Kanatani, Geometric information criterion for model selection, International Journal of Computer Vision 26 (1998) 171–189.
[10] K. Kanatani, Motion segmentation by subspace separation: Model selection and reliability evaluation, International Journal of Image Graphics 2 (2002) 179–197.
[11] K. Kanatani, Uncertainty modeling and model selection for geometric inference, IEEE Transactions on Pattern Analysis and Machine Intelligence 26 (2004) 1307–1319.
[12] K. Kanatani, Geometric BIC, IEICE Transactions on Information and Systems E93-D (2010) 144–151.
[13] K. Kanatani, H. Niitsuma, Optimal computation of 3-D similarity: Gauss-Newton vs. Gauss-Helmert, Computational Statistics and Data Analysis 56 (2012) 4470–4483.
[14] K. Kanatani, Y. Sugaya, Performance evaluation of iterative geometric fitting algorithms, Computational Statistics and Data Analysis 52 (2007) 1208–1222.
[15] K. Kanatani, Y. Sugaya, Compact fundamental matrix computation, IPSJ Transactions on Computer Vision and Applications 2 (2010) 59–70.
[16] K. Kanatani, Y. Sugaya, H. Niitsuma, Triangulation from two views revisited: Hartley-Sturm vs. optimal correction, in: Proceedings of the 19th British Machine Vision Conference, 2008, pp. 173–182.
[17] Y. Kanazawa, K. Kanatani Infinity and planarity test for stereo vision, IEICE Transactions on Information and Systems E80-D (1997), 774–779.
[18] Y. Kanazawa, K. Kanatani, Stabilizing image mosaicing by model selection, in: Pollefeys, M., Van Gool, L., Zisserman, A., Fitzgibbon, A. (Eds.), 3D Structure from Images–SMILE 2000, Springer, Berlin, 2001, pp. 35–51.
[19] Y. Kanazawa, K. Kanatani, Robust image matching preserving global consistency, in: Proceedings of the Sixth Asian Conference on Computer Vision, vol. 2, 2004, pp. 1128–1133.
[20] C. Matsunaga, K. Kanatani, Calibration of a moving camera using a planar pattern: optimal computation, reliability evaluation and stabilization by model selection, in: Proceedings of the Seventh European Conference on Computer Vision, vol.2, 2000, pp.595–609.
[21] H. Niitsuma, K. Kanatani, Optimal computation of 3-D rotation under inhomogeneous anisotropic noise, in: Proceedings of the 12th IAPR Conference on Machine Vision Applications, 2011, pp. 112–115.
[22] N. Ohta, K. Kanatani, Moving object detection from optical flow without empirical thresholds, IEICE Transactions on Information and Systems E81-D (1998) 243–245.
[23] W.H. Press, S.A. Teukolsky, W.T. Vetterling, B.P. Flannery, Numerical Recipes in C: The Art of Scientific Computing, 2nd ed., Cambridge University Press, Cambridge, 1992.
[24] J. Rissanen, Stochastic Complexity in Statistical Inquiry, World Scientific, Singapore, 1989.
[25] G. Schwarz, Estimating the dimension of a model, Annals of Statistics 6 (1987), 461–464.
[26] Y. Sugaya, K. Kanatani, Multi-stage optimization for multi-body motion segmentation, IEICE Transactions on Information and Systems E87 (2004), 1935–1942.
[27] I. Triono, N. Ohta, K. Kanatani, Automatic recognition of regular figures by geometric AIC, IEICE Transactions on Information and Systems E81 (1998) 246–248.

Kenichi Kanatani received his B.E., M.S., and Ph.D. in applied mathematics from the University of Tokyo in 1972, 1974 and 1979, respectively. After serving as Professor of computer science at Gunma University, Gunma, Japan, he is currently Professor of computer science at Okayama University, Okayama, Japan. He is the author of many

Kenichi Kanatani books on computer vision, including "Group-Theoretical Methods in Image Understanding," Springer, 1990, "Geometric Computation for Machine Vision," Oxford University Press, 1993, and "Statistical Optimization for Geometric Computation: Theory and Practice," Elsevier 1996. He is an IEEE Fellow.

Chikara Matsunaga received his B.E. and M.S. in electronic engineering from Muroran Institute of Technology, Hokkaido, Japan, in 1988 and 1990, respectively, and his Ph.D. in computer science from Gunma University, Gunma, Japan, in 2001. Since 1990, he has been working for FOR-A Co., Ltd., Japan, where he is engaged in professional video equipment development and image processing and computer vision research.